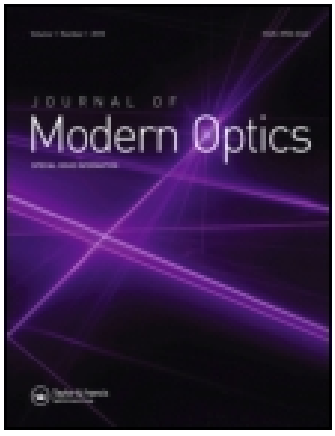

Journal of Modern Optics
Publication details, including instructions for authors and subscription information:
http://www.tandfonline.com/loi/tmop20

Numerical implementation of generalized Coddington equations for ophthalmic lens design

P. Rojo[ab], S. Royo[a], J. Ramírez[c] & I. Madariaga[c]

[a] UPC-CD6, Center for Sensor, Instruments and Systems Development, Universitat Politècnica de Catalunya, Rambla Sant Nebridi 10 Terrassa E08222, Spain

[b] Vallès Oftalmologia Recerca VO-R. Hospital General de Catalunya. 4th floor Green building, Room 387. C/Pedro I Pons,1 Sant Cugat del Vallès E08195, Spain

[c] Industrias de Óptica Prats, Dr Josep Castells, 4, S.Boi de Llobregat, E08830 Spain

Published online: 30 Jan 2014.

To cite this article: P. Rojo, S. Royo, J. Ramírez & I. Madariaga (2014) Numerical implementation of generalized Coddington equations for ophthalmic lens design, Journal of Modern Optics, 61:3, 204-214, DOI: 10.1080/09500340.2013.878964

To link to this article: http://dx.doi.org/10.1080/09500340.2013.878964

Journal of Modern Optics, 2014
Vol. 61, No. 3, 204–214, http://dx.doi.org/10.1080/09500340.2013.878964

Numerical implementation of generalized Coddington equations for ophthalmic lens design

P. Rojo[a,b], S. Royo[a]*, J. Ramírez[c] and I. Madariaga[c]

[a]*UPC-CD6, Center for Sensor, Instruments and Systems Development, Universitat Politècnica de Catalunya, Rambla Sant Nebridi 10 Terrassa E08222, Spain;* [b]*Vallès Oftalmologia Recerca VO-R. Hospital General de Catalunya. 4th floor Green building, Room 387. C/Pedro I Pons,1 Sant Cugat del Vallès E08195, Spain;* [c]*Industrias de Óptica Prats, Dr Josep Castells, 4, S.Boi de Llobregat, E08830 Spain*

(*Received 19 September 2013; accepted 18 December 2013*)

A method for general implementation in any software platform of the generalized Coddington equations is presented, developed, and validated within a Matlab environment. The ophthalmic lens design strategy is presented thoroughly, and the basic concepts of generalized ray tracing are introduced. The methodology for ray tracing is shown to include two inter-related processes. Firstly, finite ray tracing is used to provide the main direction of propagation of the considered ray at the incidence point of interest. Afterwards, generalized ray tracing provides the principal curvatures of the local wavefront at that point, and its orientation after being refracted by the lens. The curvature values of the local wavefront are interpreted as the sagital and tangential powers of the lens at the point of interest. The proposed approach is validated using a double-check of the calculated lens performance in the spherical lens case: while finite ray tracing is validated using a commercial ray tracing software, generalized ray tracing is validated using a software application for ophthalmic lens design based on the classical version of Coddington equations. Equations of the complete tracing process are developed in detail for the case of generic astigmatic ophthalmic lenses as an example. Three-dimensional representation of the sagital and tangential powers of the ophthalmic lens at all directions of gaze then becomes possible, and results are presented for lenses with different geometries.

Keywords: Coddington equation; generalized ray tracing; ophthalmic lens

1. Introduction

1.1. Overview of the ophthalmic lens design problem

The basic theory of ophthalmic lens design is based on the fundamental laws of geometrical optics, and dominated exclusively by refraction effects. An ophthalmic lens is an optical element that properly modifies the curvature of the wavefront before it reaches the eye, in order to compensate for the eye's refractive error and form a sharp image of the observed object on the eye's fovea, at the retina. The ophthalmic lens is a very simple optical element defined by a few geometrical parameters that can be changed and adjusted to obtain the desired power of the lens. In ophthalmic optics, 'power' always refers to back vertex power, namely, the inverse of the distance from the back vertex of the lens to its image focal point. As far as ophthalmic lenses are manufactured in almost all cases with a meniscus shape, the curvature of the two available surfaces defines a first surface with positive power and a second one with negative power. There are endless possibilities to combine these parameters with each other and still get the same total power of the lens. However, the different combinations cause different performance of the lens off-axis [1–3].

The compensation condition is defined on-axis, as the coincidence of the image focal point of the ophthalmic lens with the remote point of the eye, which is the object point conjugated with the fovea in a non-accommodated eye. The classical theory of ophthalmic lens design proposes that the condition of compensation of the refractive error should be maintained over the surface defined by the position of the remote point at all directions of gaze [2, 4–6]. Although the aperture of the eye may be considered small in general, this ideal condition is impossible to attain in practice, due to the lack of degrees of freedom in the lens–eye system, where in the case of spherical surfaces only the curvature of one surface may be chosen by the designer. Aspherical surfaces enable one additional degree of freedom when the conic constant is considered.

For directions of gaze outside the optical axis aperture aberrations are usually neglected, but the effect of field aberrations needs be considered. The image of an object blurs due to the presence of oblique astigmatism, and its associated changes in effective power. The image of eccentric object points generates both a tangential and a sagital focal lines which change with the oblique angle of gaze (Figure 1). The different classical solutions for spherical lens design vary in the criteria to manage this

*Corresponding author. Email: santiago.royo@upc.edu

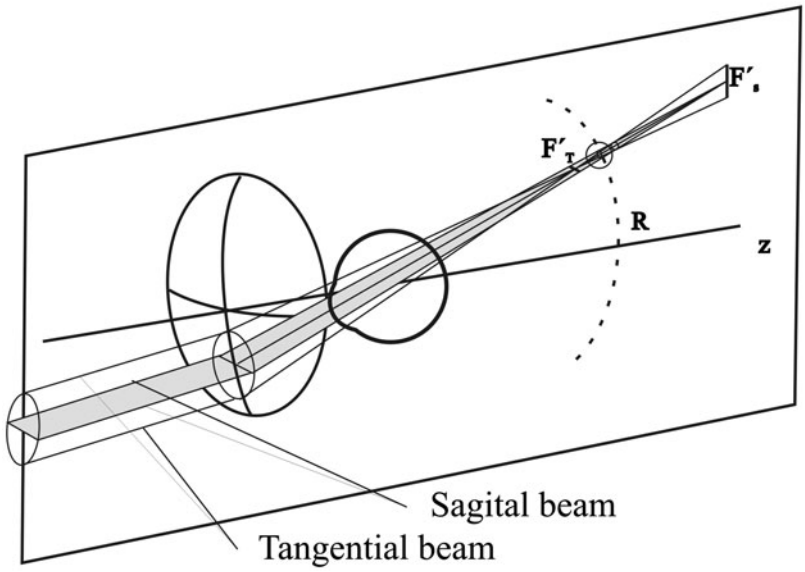

Figure 1. Oblique astigmatism in an off-axis object point for the lens–eye system.

focus shift across the field, changing the curvature of a single surface. Percival lenses, point-focal lenses [4] and minimal tangential error lenses are some of the solutions used in practice [7].

1.2. Generalized Coddington equations

When a narrow bundle of rays of light created by an eccentric object point arrives to the lens-eye system, the eye rotates around its center of rotation to look through eccentric points of the lens. These are the conditions defined for the application of the equations developed by Coddington in the early nineteenth Century [8]. Coddington equations are used to calculate the analytical solutions for the tangential and sagital foci derived from oblique astigmatism generated by a spherical refracting surface whose surface normal is tilted relative to the principal ray of the incoming narrow bundle of rays [2].

Coddington equations for the position of the sagital and tangential focus are written as:

$$n'/s' - n/s = (n'\cos i' - n\cos i)/r, \quad (1)$$

$$((n'\cos^2 i')/t' - (n\cos^2 i)/t) = (n'\cos i' - n\cos i)/r, \quad (2)$$

where r is the radius of curvature of the refracting spherical surface, n the refractive index in the incident medium, n' the refractive index in the refracted medium, i the angle of incidence of the chief ray, and i' its angle of refraction, with all angles calculated relative to the normal to the surface. s and t are the object distances and s' and t' are the image distances to the sagital and tangential foci, respectively. They are, thus, two-dimensional (2D) equations which describe the behavior of the ray fan in the incidence plane.

Different generalizations have been proposed to these equations, initially proposed for spherical surfaces, in order to adapt them to surfaces with arbitrary shapes [9,10], yielding what has been known as generalized Coddington equations (GCE). The main contributions in this point have been related to the inclusion of differential geometry aspects in Coddington approach, which has allowed an alternative derivation of the classical equations [11–13]. A matrix version of the GCE has also been proposed, and its equivalence with Equations (1) and (2) established [14].

In the approach we will follow, each ray traced through an optical system is associated to a local wavefront which propagates through the optical system. According to this, a pencil of light can be considered as composed of a principal ray and a wavefront in its neighborhood. The propagation of the wavefront in the neighborhood of the principal ray through the lens-eye system is used for the evaluation of the performance of the lens [15,16]. This approach is usually referred to as generalized ray tracing (GRT), and sometimes as wavefront tracing. In contrast to conventional ray tracing, in GRT the key parameters are the shape and orientation of the local wavefront in the vicinity of its principal ray. This view is particularly useful in the design of ophthalmic lenses, where the optical system has its beam size limited by the aperture of the pupil, and the degrees of freedom reduce to the local curvatures of the surfaces of the lens. Using wavefront tracing in a dedicated environment allows a much faster performance of the software than the use of the conventional, intensive ray tracing approaches used in general optical system design, where the problem to be solved is essentially different.

Other approaches have involved reconsidering Equations (1) and (2) to fix the tangential and sagital focal length of any ray contained in the tangential plane, and not just the main beam, deriving formulas for more efficient evaluation of the aberrations [17]. Other authors have proposed considering the refraction of a wavefront by a powered element as the action of an operator acting on the wavefront [18], introducing the concept of vergence operators. Lately, a general method to generate equations for refraction from wavefront aberrations of any local order for any incidence condition has been proposed [19]. It is thus clear that Coddington equations play a central role in ophthalmic lens design and are still subject of active research, with optimization of the foveal vision conditions for all directions of gaze as the objective [2,4,20].

Dedicated tracing software for ophthalmic lens design has a number of relevant applications which may be useful to evaluate different issues on lens performance. Effects like wrong positioning of the lens, tilt of the lens on the spectacles (pantoscopic or faceform), optimum base curve, asphericity or free-form surfacing affect significantly the off-axis behavior of the ophthalmic lens. Furthermore, at present it is hard to discuss the performance of a given lens design, method or procedure claimed to be introduced by the industry without some general-purpose calculation tool. The existence of a tool to evaluate real lens performance in wear conditions is, subsequently, each time more relevant both for the student, the lens designer and the optometrist.

The aim of this work is to describe in detail the numerical implementation of the equations proposed for ophthalmic lens design using the GRT approach [13,14,21]. The work has been divided in five sections plus this introduction. Firstly, the theoretical framework of the work is presented, starting with the process of finite ray tracing (FRT), which provides the exact path of the principal ray. Next, the concept of GRT and its principal equations are discussed in detail. At this point, the principal curvatures and directions of the refracted wavefront can be calculated for all directions of gaze. Then we will present how to evaluate the performance of an ophthalmic lens, using the developed equations of finite ray tracing and GRT. The detailed development of FRT and GRT equations in the case of an astigmatic ophthalmic lens is presented in an Appendix to this paper, to improve its readability without penalizing its completeness. Finally, the full procedure becomes validated in a typical ophthalmic lens using Beam 4, a commercial ray tracing software, and Primer, a software for ophthalmic lens design based on the classical Coddington equations [7]. Some results obtained for different lens geometries are then presented to show the potential of the software. A final section will draw out the main conclusions of our work. To the best of our knowledge, this is the first time that a detailed implementation of GRT procedures has been presented.

2. Theoretical framework

2.1. *Finite rays and finite ray tracing*

When rays are traced from a point of the object plane without making the approximations of Gaussian optics, i.e. when they are traced exactly according to Snell's law, they are called finite rays. The process of tracing them is known as finite ray tracing (FRT), which is essentially an iterative sequence of transfer and refraction operations. Transfer takes a ray from where it leaves one optical surface to where it meets the next one, so in homogeneous media it reduces to linear propagation. Refraction finds the new direction of the ray once it has passed through the surface of interest [22].

The refraction process is governed by Snell's law. Let S be a surface that separates two media of constant refractive index n and n'. An incident ray, with a direction vector $\boldsymbol{r}$, intercepts the refracting surface at some point P, giving rise to a refracted ray whose direction vector is $\boldsymbol{r}'$ (Figure 2).

The relationship of the incident and refracted ray and $\boldsymbol{n}$, the unit normal to the refracting surface at P, is given by the vector form of Snell's law:

$$n'(\boldsymbol{r}' \times \boldsymbol{n}) = n(\boldsymbol{r} \times \boldsymbol{n}) \tag{3}$$

or

$$\boldsymbol{r}' \times \boldsymbol{n} = \mu(\boldsymbol{r} \times \boldsymbol{n}), \tag{4}$$

where μ is the ratio of the refractive indices before and after surface S. The well-known scalar version is thus simply

$$\sin i' = \mu \sin i, \tag{5}$$

where i and i' are the angles of incidence and refraction. In vector form we can write

$$(\boldsymbol{r}' - \mu\boldsymbol{r}) \times \boldsymbol{n} = 0, \tag{6}$$

as vectors $(\boldsymbol{r}' - \mu\boldsymbol{r})$ and $\boldsymbol{n}$ are parallel. Therefore, a scalar quantity γ such that $(\boldsymbol{r}' - \mu\boldsymbol{r}) = \gamma\boldsymbol{n}$ may be found.

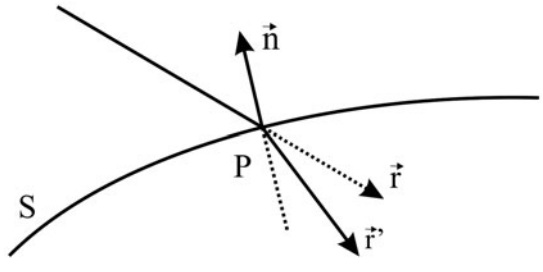

Figure 2. Outline for FRT. **n** is the normal to S at P.

The vector direction of the refracted ray can be expressed as a linear combination of the incident ray vector and the surface normal

$$\boldsymbol{r}' = \mu \boldsymbol{r} + \gamma \boldsymbol{n}, \tag{7}$$

which is the vectorial ray tracing formula for refraction.

Finally, γ must be determined. Since $\boldsymbol{r}$, $\boldsymbol{r}'$, and $\boldsymbol{n}$ are unit vectors, the square of the above equation yields

$$1 = \mu^2 + \gamma^2 + 2\mu\gamma(\boldsymbol{r} \cdot \boldsymbol{n}), \tag{8}$$

which is a quadratic equation in γ whose solution may be written as

$$\gamma = \mu(r \cdot n) + \left\{1 - \mu^2[1 - (r \cdot n)^2]\right\}^{1/2} = -\mu \cos i + \cos i'. \tag{9}$$

2.2. Generalized ray tracing

Generalized ray tracing (GRT) procedures assume that each ray traced through an optical system may be associated with a local wavefront that propagates through it This local wavefront present in the neighborhood of the principal ray has well-defined geometric properties. In general, it will have two principal directions and two principal curvatures at the point where the ray intercepts the wavefront. The principal directions are given by the two orthogonal vectors tangent to the wavefront at the ray intersection, for which the geodesic curvatures assume maximum and minimum values. The principal curvatures are these two extreme values of geodesic curvature. GRT explains what happens to the principal directions and principal curvatures of the wavefront after transfer and refraction [13,14,21].

For transfer, the principal directions of the local wavefront are unchanged, and their centers of curvature remain fixed. Refraction is depicted graphically in Figure 3(*a*). Let W and W' represent the incident and refracted local wavefronts, respectively. Let $\boldsymbol{r}$ and $\boldsymbol{r}'$ represent the direction vectors of an incident and a refracted ray. Let P be the point of intersection of these rays on the refracting surface S and let the normal to the refracting surface at that point be $\boldsymbol{n}$. We next introduce three coordinate systems associated with the incident wavefront, the refracting surface, and the refracted wavefront (Figure 3(*b*)).

Let's define a unit vector $\boldsymbol{p}$ such as

$$\boldsymbol{p} = \boldsymbol{r} \times \boldsymbol{n} / \sin i. \tag{10}$$

$\boldsymbol{p}$ is perpendicular to $\boldsymbol{r}$, $\boldsymbol{n}$, and $\boldsymbol{r}'$. In other words, $\boldsymbol{p}$ is perpendicular to the plane of incidence. Moreover, since $\boldsymbol{r}$ is perpendicular to W, $\boldsymbol{n}$ to S, and $\boldsymbol{r}'$ to W', $\boldsymbol{p}$ is a tangent vector to the two wavefronts and to the refracting surface.

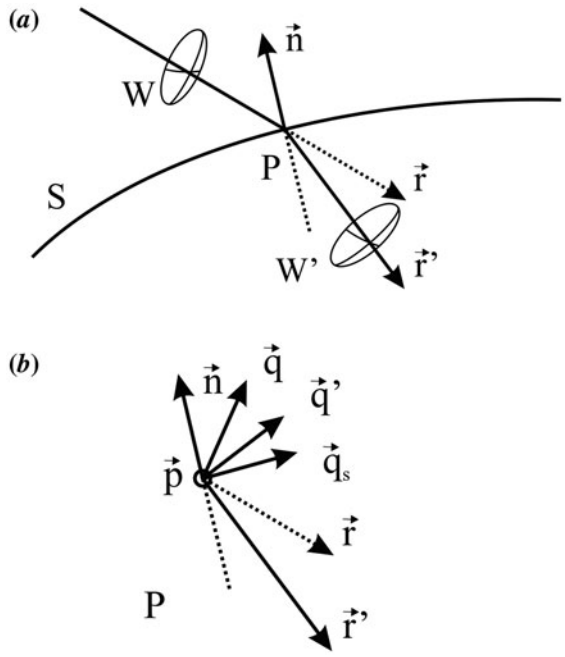

Figure 3. GRT schematics. (*a*) Representation including the incoming and outgoing wavefronts W and W'. (*b*) Representation of the full set of vectors involved in the calculations at P, the point of incidence of the ray on S.

We define three additional unit vectors,

$$\boldsymbol{q} = \boldsymbol{r} \times \boldsymbol{p}, \tag{11}$$

$$\boldsymbol{q}_s = \boldsymbol{n} \times \boldsymbol{p}, \tag{12}$$

$$\boldsymbol{q}' = \boldsymbol{r}' \times \boldsymbol{p}, \tag{13}$$

each perpendicular to $\boldsymbol{p}$ and each tangent to the appropriate surface. We now have a set of three orthogonal unit vectors associated with each surface:

$$W : \boldsymbol{r}, \boldsymbol{p}, \boldsymbol{q}; \quad S : \boldsymbol{n}, \boldsymbol{p}, \boldsymbol{q}_s; \quad W' : \boldsymbol{r}', \boldsymbol{p}, \boldsymbol{q}'. \tag{14}$$

Each set of vectors is orthogonal, and then, considering the vectors in W,

$$\boldsymbol{q} = \boldsymbol{r} \times \boldsymbol{p}; \quad \boldsymbol{r} = \boldsymbol{p} \times \boldsymbol{q}; \quad \boldsymbol{p} = \boldsymbol{q} \times \boldsymbol{r}, \tag{15}$$

and in an equivalent manner for S and W', the other surfaces of interest. The pair of principal curvatures of the incident wavefront W, of the refracted wavefront W', and of the surface S are labeled as ρ_ξ, ρ_μ, ρ'_ξ, ρ'_η, $\rho_{\xi s}$, $\rho_{\eta s}$, respectively. The directions of these principal curvatures are given by the vectors $\boldsymbol{t}$, $\boldsymbol{t}'$, and $\boldsymbol{t}_s$. The angles between the vectors $\boldsymbol{t}$, $\boldsymbol{t}'$, and $\boldsymbol{t}_s$ and $\boldsymbol{p}$ are $\boldsymbol{\theta}$, $\boldsymbol{\theta}'$, and $\boldsymbol{\theta}_s$, given by:

$$\cos\theta = \boldsymbol{t} \cdot \boldsymbol{p}; \quad \cos\theta' = \boldsymbol{t}' \cdot \boldsymbol{p}; \quad \cos\theta_s = \boldsymbol{t}_s \cdot \boldsymbol{p}. \tag{16}$$

In this way, the normal curvatures relative to the defined coordinate system and the related torsion for the incident wavefront are defined by

$$1/\rho_u = (1/\rho_\xi)\cos^2\theta + (1/\rho_\eta)\sin^2\theta, \tag{17}$$

$$1/\rho_v = (1/\rho_\xi)\sin^2\theta + (1/\rho_\eta)\cos^2\theta, \tag{18}$$

$$(2/\sigma) = (1/\rho_\xi - 1/\rho_\eta)\sin 2\theta, \tag{19}$$

where ρ_u is the incident wavefront curvature on the $\boldsymbol{p}$ direction, ρ_v is the incident wavefront curvature on the $\boldsymbol{q}$ direction, and σ is the torsion.

Likewise, the curvatures of the refracting surface and of the refracted wavefront in the defined local coordinate systems can be calculated yielding equivalent ρ'_u, ρ'_v, ρ_{us}, ρ_{vs}. The inverse relationships may also be obtained. Given the curvatures of two orthogonal normal sections, the quantity σ, and the angle between the principal directions and the normal sections, θ, the principal curvatures may be calculated using:

$$1/\rho_\xi = (1/\rho_u)\cos^2\theta + (1/\rho_v)\sin^2\theta + (2/\sigma)\sin\theta\cos\theta, \tag{20}$$

$$1/\rho_\eta = (1/\rho_u)\sin^2\theta + (1/\rho_v)\cos^2\theta - (2/\sigma)\sin\theta\cos\theta, \tag{21}$$

$$\tan 2\theta = (2/\sigma)/(1/\rho_v - 1/\rho_u), \tag{22}$$

and the vector $\boldsymbol{t}$ is:

$$\boldsymbol{t} = \boldsymbol{p}\cos\theta + \boldsymbol{q}\sin\theta. \tag{23}$$

Now, the set of generalized ray tracing equations can be presented. These equations are obtained from the directional derivative of the vector form of Snell's law and from the Frenet equations for space curves [13]. GRT equations provide the refracted wavefront curvatures on the $\boldsymbol{p}$ direction (ρ'_u) and on the $\boldsymbol{q}$ direction (ρ'_v) and σ', the torsion of the refracted wavefront, using

$$1/\rho'_u = \mu/\rho_u + (\gamma/\rho_{us}), \tag{24}$$

$$\cos i'/\sigma' = (\mu\cos i/\sigma) + (\gamma/\sigma_s), \tag{25}$$

$$\cos^2 i/\rho'_v = (\mu\cos^2 i/\rho_v) + (\gamma/\rho_{vs}). \tag{26}$$

3. Ray tracing equations for ophthalmic lens design

Let's now take a brief look onto the global ray tracing procedure used in ophthalmic lens design. The list of equations used for the implementation of GRT procedures in the case of an astigmatic ophthalmic lens is developed in detail in the Appendix, while in this section only a general description of the procedure will be presented.

The main assumption in ophthalmic lens design is considering that the optical system behaves as if the eye had a fixed aperture with the dimension of the pupil size placed at the center of rotation of the eye. This concept significantly simplifies the lens design problem, as the optical system of the eye is ignored, replacing it by a remote surface and an aperture at the center of rotation of the eye [1,2,4] (Figure 4). The remote surface is the continuous surface described by the remote point when the eye rotates and is the place where the best focus of the lens should ideally be present for all directions of gaze.

As mentioned, the method to evaluate ophthalmic lens performance includes a FRT process followed by a GRT procedure. For the FRT part, we will be interested in the reverse path followed by the rays starting at the center of rotation of the eye and reaching the posterior surface of the lens, and, afterwards, the object space. The path followed by this ray is determined using Equation (7). Each direction of gaze is thus characterized by a given finite ray (Figure 5(*a*)).

Once we have traced the principal ray direction, the path of the ray will be inverted, the system will be rotated backwards to its initial position and GRT algorithms will be applied. This second step will calculate the effects on wavefront geometry as the beam travels through each surface of the lens with a particular inclination (Figure 5(*b*)). Such inclination is chosen to evaluate a particular direction of gaze and is determined by the calculated direction of the ray in the previous FRT step. The wavefront in the neighborhood of this ray will have two principal directions and two principal curvatures at the point where the ray intercepts the wavefront. GRT will evaluate how these directions and curvatures change when the wavefront crosses the lens using Equations (24)–(26). The centers of curvature for such principal curvatures of the wavefront are equivalent to the sagital and tangential focus positions in Equations (1) and (2).

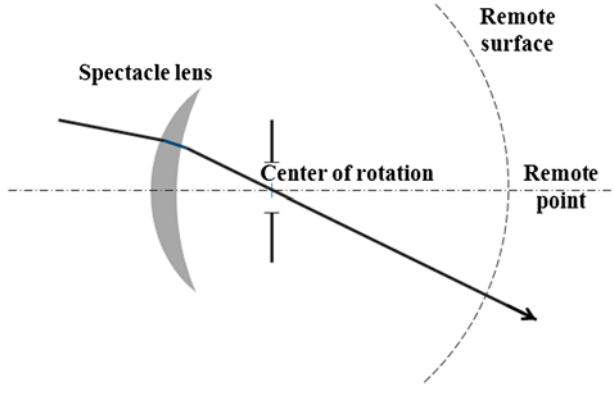

Figure 4. Basic layout for classical ophthalmic lens design. (The colour version of this figure is included in the online version of the journal.)

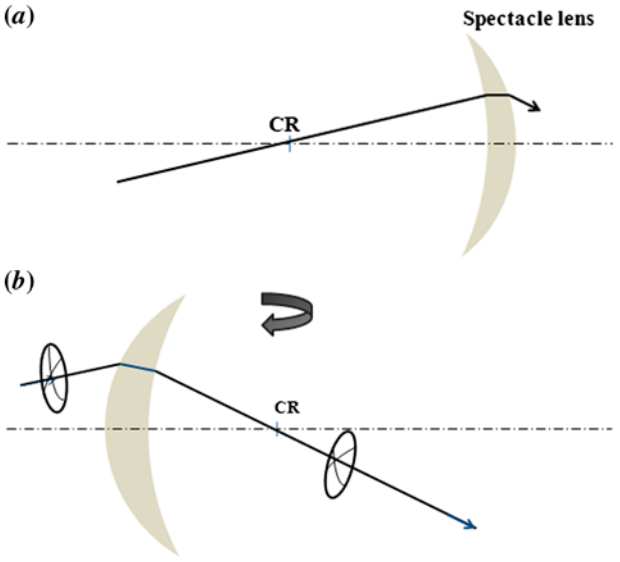

Figure 5. (*a*) Reverse ray path for a given direction of gaze. The system has been rotated 180° relative to an imaginary vertical axis. The ray passes through the center of rotation (CR) of the eye to arrive to the posterior surface of the spectacle lens. (*b*) GRT step will calculate the effects on wavefront geometry as the beam travels through each surface. (The colour version of this figure is included in the online version of the journal.)

4. Validation

The validation of the equations and its software implementation is divided in two parts, following the tracing scheme depicted. Firstly we will validate the principal ray path of the wavefront when the inverse path of the ray is considered by comparison of our Matlab® implementation with the results obtained using Beam 4®, a commercial exact ray tracing software from Stellar® software, which enables ray by ray slope calculation and the exact calculation of the intersection point of the surface for each ray. A similar validation could be performed using any usual software optical design package, like Zemax® or OSLO®. The second part is the validation of the refracted wavefront curvatures after the wavefront has passed through the lens. The validation of the wavefront curvatures is compared with Primer, a software for ophthalmic lens design based on the classical version of Coddington equations [22].

For validation we will consider a spherical lens with +2.00 D back vertex power, suitable for moderate hypermetropia, with center thickness of 3 mm, refractive index of 1.5, radius of the anterior surface 71.44 mm, and radius of the posterior surface 98.05 mm. The center of rotation of the eye is located 27 mm away from the posterior surface of the lens. The three-dimensional (3D) sagital and tangential focal distribution will be presented in the results section. Equivalent results for validation are obtained in all cases. The director cosines of the ray and the parameters of the lens are introduced in the application to obtain the point of incidence of any ray on each surface of the lens and the director cosines for this ray after each refraction.

The same optical system is moved to Beam 4 to validate the values of the coordinates of the point of incidence on each surface and the director cosines of the ray after refraction. Figure 6 show values obtained with Matlab and Beam 4, when the ray arrives to the second surface of the lens and is refracted. The comparison of

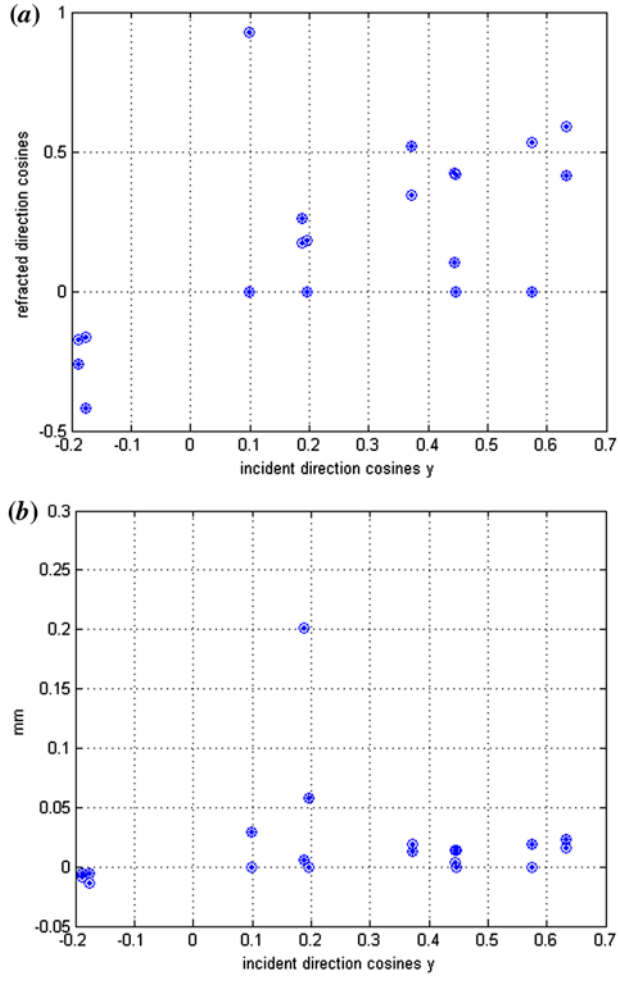

Figure 6. (*a*) Values obtained from Matlab (circle) and from Beam 4 (cross) for the X director cosines of the refracted ray on the anterior surface of the lens. Values obtained from Matlab (dot) and from Beam 4 (plus) for the Y director cosines of the refracted ray on the anterior surface of the lens. (*b*) X local coordinate values obtained from Matlab (dotted) and from Beam 4 (circle) for the point of incidence of each ray on the anterior surface of the lens. The same for Y local coordinate values (Matlab (cross) and Beam 4 (circle)) and also for Z local coordinate values (Matlab (*) and Beam 4 (o)). Coincidence is complete. (The colour version of this figure is included in the online version of the journal.)

Table 1. Tangential and sagital powers obtained by generalized ray tracing (left in each column) and by classical Coddington equations (right in each column) for different degrees of eccentricity.

Rotation angle of the eye (°)	Tangential power (diopters)	Sagital power (diopters)
5	2.0001/2.00	1.9981/2.00
10	2.0002/2.00	1.9924/1.99
15	1.999/2.00	1.9823/1.98
20	1.9944/1.99	1.9674/1.97
25	1.9834/1.98	1.9467/1.95
30	1.9615/1.96	1.9189/1.92
35	1.9228/1.92	1.8828/1.88
40	1.86/1.86	1.8368/1.84

the refracted director cosines in x and y (Figure 6(*a*))and the coordinates of the point of incidence of the ray on the second surface of the lens (Figure 6(*b*)) in both applications are presented, showing full coincidence.

To validate GRT algorithms, wavefronts with principal rays contained on the tangential plane are sent to the previously discussed lens. The associated wavefronts are chosen in order to make a validation using the classical version of Coddington equations, where a 2D problem is considered. Table 1 show the values obtained for different angles of rotation of the eye (i.e. directions of gaze) for the tangential and sagital powers in front the values obtained by an application using the classical Coddington equations. Calculated values are placed at the left in each column, while available classical Coddington values are placed at the right. Figure 7 presents these solutions graphically.

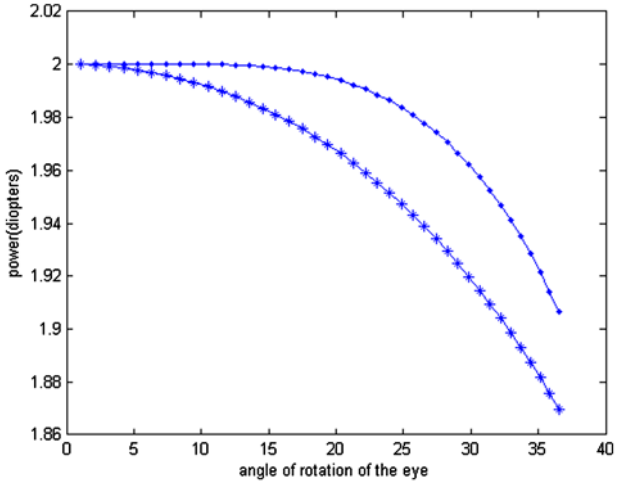

Figure 7. Tangential (.) and sagital powers (*) obtained by classical Coddington equations and tangential power and sagital power (lines) obtained by generalized ray tracing for different directions of gaze (degrees) for the +2.00 D lens described. The center of rotation of the eye is 27 mm away from the posterior surface of the lens. Coincidence is complete. (The colour version of this figure is included in the online version of the journal.)

5. Results

A software implementation of the equations as Matlab® functions makes possible a three-dimensional representation of the tangential and sagital powers of ophthalmic lenses with different geometries for different directions of gaze.

Figure 8 shows two examples for spherical lenses. Figure 8(*a*) shows the power in all directions of gaze for the +2.00 D back vertex power lens described in the validation Section. Figure 8(*b*) represents the tangential and sagital powers for a lens with a back vertex power of −8.00 D, suitable for a myopic patient, with central thickness of 1 mm, index of refraction 1.7, radius of the

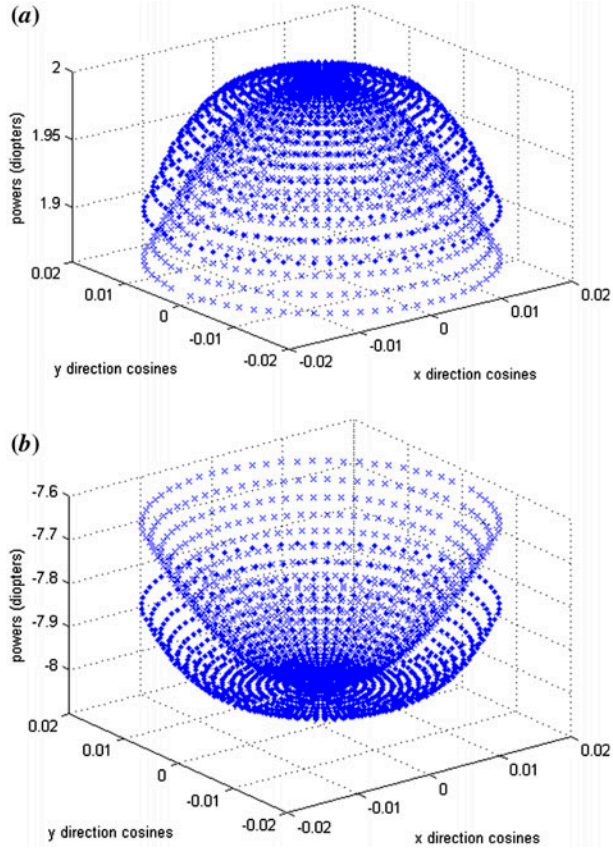

Figure 8. (*a*) Tangential (exterior cup) and sagital (interior cup) powers for the +2.00 D back vertex power lens described in the text. (*b*) Tangential (exterior cup) and sagital (interior cup) powers for a −8.00 D back vertex power lens described in the text. The vertical axis contains the power values expressed in diopters. x and y director cosines determine a particular direction of gaze in space. (The colour version of this figure is included in the online version of the journal.)

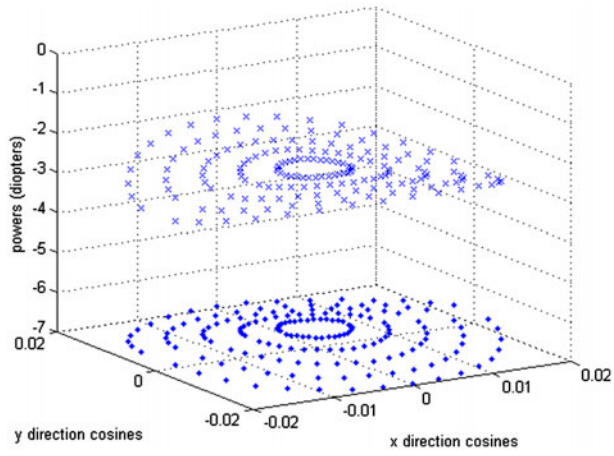

Figure 9. Maximum (diamond) and minimum (cross) absolute value power for the astigmatic 180°–4.00–2.50 back vertex power lens described in the text. The vertical axis contains the power values expressed in diopters. x and y director cosines determine a particular direction of gaze in space. The difference between power values reflects the presence of cylinder. (The colour version of this figure is included in the online version of the journal.)

anterior surface of the lens 215.38 mm, and radius of the posterior surface 62.19 mm. The center of rotation of the eye is situated 30 mm away from the posterior surface of the lens. The vertical axis contains the power values expressed in diopters. The horizontal axis contains y direction and x direction cosines for a particular direction of gaze.

Finally, Figure 9 shows the three-dimensional off-axis performance of an astigmatic lens. In this case, the convex surface of the lens is spherical and the concave surface is toroidal. The figure shows the power in all directions of gaze for a lens of 180°–4.00–2.50 back vertex power, center thickness of 1.60 mm, refractive index of 1.579, radius of the anterior surface 298.50 mm, and principal radii at the posterior toroidal surface of 132.44 and 70.17 mm. The center of rotation of the eye is located 27 mm away from the posterior surface of the lens. The vertical axis contains the power values expressed in diopters. Horizontal axis contains y direction and x direction cosines for a particular direction of gaze. The large difference between power values reflects the presence of a large cylinder.

6. Conclusions

The theoretical foundations for the elaboration of a tool including the numerical implementation of the modern principles of FRT and GRT has been detailed, developed and validated. The combination of FRT and GRT outperforms in speed the classical intensive ray tracing procedures used in opto-mechanical system design and is better suited to the specificities of the ophthalmic lens design problem.

In the presented approach, a finite ray trace is first applied to know the exact path of the principal ray of the wavefront. Then, GRT is applied to obtain the principal curvatures of the refracted local wavefront through the lens, which are the tangential and sagital lens powers at the considered direction of gaze. The method for performing the ray tracing has been presented in detail, as the equations to be implemented numerically, leaving just simple software coding in the desired platform to make them fully functional. A complete derivation of the equations for GRT in the case of a toroidal lens is presented in an Appendix to the paper. The results of the proposed implementation have been validated using a commercial ray tracing software, for the finite ray tracing part. For the GRT algorithms, wavefronts with their principal ray contained on the tangential plane have been used and compared to the results obtained using the classical version of Coddington equations. Validation has shown complete coincidence of the results.

The approach allows a full 3D representation of the off-axis tangential and sagital powers of the lens. The user has now the capability to evaluate the effective power of a given design, or its performance in its real position of use (for lenses tilted with pantoscopic or face-form angles, or its combination). The presented approach has shown its usefulness for the analysis of the performance of the off-axis performance of ophthalmic lenses of different geometries.

References

[1] Fannin, T.; Grosvenor, T. *Clinical Optics*; Butterworth-Heinemann: Boston, **1996**.
[2] Jalie, M. *The Principles of Ophthalmic Lenses*; The Association of Dispensing Opticians: London, **1984**.
[3] Salvadó, J.; Fransoy, B.; *Tecnología Óptica. Lentes Oftálmicas, Diseño y Adaptación*; Edicions UPC: Barcelona, **1996**.
[4] Atchison, D. *Aust. J. Optom.* **1984,** *67*, 97–107.
[5] Grosvenor, T. *Optometría de Atención Primaria*; MASSON: Barcelona, **2004**; pp 391–401.
[6] Atchison, D.; Tame, S. *Clin. Exp. Optom.* **1992,** *75*, 210–217.
[7] Jalie, M. *Ophthalmic Lenses and Dispensing*; Butterworth-Heinemann: UK, **2003**.
[8] Kingslake, R. *Opt. Photonics News* **1994,** *5* (8), 20–23.
[9] Gullstrand, A. *K. Sven. Ventenskapsakad. Akad*, **1906,** *XLI*, 1–139.
[10] Sturm, J. *J. Math. Pure Appl.* **1838,** *3*, 357–361.
[11] Keating, M. *Optom. Vision Sci.* **1993,** *70*, 785–791.
[12] Kneisly, J. II. *J. Opt. Soc. Am.* **1964,** *54*, 229–235.
[13] Burkhard, D., Shealy, D. *Appl. Opt.* **1981,** *20*, 897–909.
[14] Landgrave, J.; Moya-Cessa, J. *J. Opt. Soc. Am.* **1996,** *13*, 1637–1644.
[15] Stavroudis, O. *J. Opt. Soc. Am.* **1976,** *66*, 1330–1333.
[16] Stavroudis, O. *The Optics of Rays, Wavefronts, and Caustics*; Academic Press: UK, **1972**; pp 149–169.

[17] Comastri, S. *J. Mod. Opt.* **2001,** *48*, 379–404.
[18] Campbell, C. *J. Opt. Soc. Am.* **2006,** *23*, 1691–1698.
[19] Esser, G.; Becken, W.; Müller, W.; Baumbach, P.; Arasa, J.; Uttenweiler, D. *J. Opt Soc. Am.* **2010,** *27*, 218–237.
[20] Atchison, D. *Appl. Opt.* **1992,** *31*, 3579–3585.
[21] Stavroudis, N.; Fronczek, R. *J. Opt. Soc. Am.* **1976,** *66*, 795–800.
[22] Welford, W. *Aberrations of Optical Systems*; Adam Hilger: Bristol, **1986**, pp 50–55.
[23] Do Carmo, M. P. *Geometría Diferencial De Curvas y Superficies*; Alianza Universidad Textos: **1990**. pp 159–173.

Appendix. Detailed generalized ray tracing equations

A1. Finite ray tracing

As commented in Section 3, we will perform first a FRT procedure in order to know the path of the principal ray at the considered direction of gaze. We will consider the ophthalmic lens to be astigmatic, with a toroidal concave surface and a spherical convex surface, in order to present a general case. To the best of our knowledge, this is the first time that this astigmatic lens case has been covered in detail in the literature.

Each surface of the lens can be parameterized in a particular coordinate system situated at the vertex of each surface. For the parameterization of the posterior surface, a torus situated at the posterior vertex of the lens has been considered (see Figure A1). It has two orthogonal radius of curvature R and r, situated at 180° and 90°, respectively. The difference between these radius expressed in diopters is the cylindrical power of the lens, or simply its cylinder.

The parametric equation in polar coordinates for this surface is:

$$s = \left\{ \begin{array}{l} x = (R - r + r\cos\varphi)\sin\theta \\ y = r\sin\varphi \\ z = -R + (r - r + r\cos\varphi)\cos\theta \end{array} \right\}, \qquad (27)$$

where $0 \le \varphi \le 2\pi$ and $0 \le \theta \le 2\pi$ and R and r are considered as absolute values.

A ray characterized by its director cosines (L, M, N) in a reference system with origin at the center of rotation of the eye is chosen for tracing (Figure A2). The center of rotation is separated from the posterior vertex of the lens a distance d. The ray arrives to the posterior surface of the lens at point P_1.

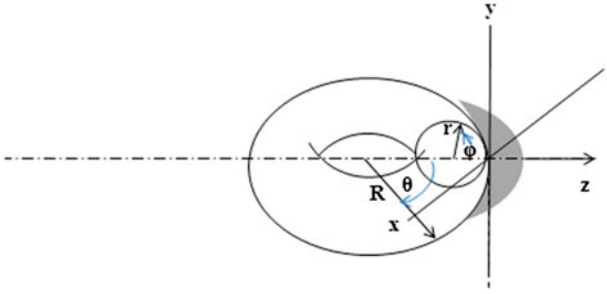

Figure A1. For the toroidal lens, a toroidal surface is considered to be situated at the posterior vertex of the lens, with two radius of curvature, R and r. The angles φ and θ will be used for the parametric equation in polar coordinates. (The colour version of this figure is included in the online version of the journal.)

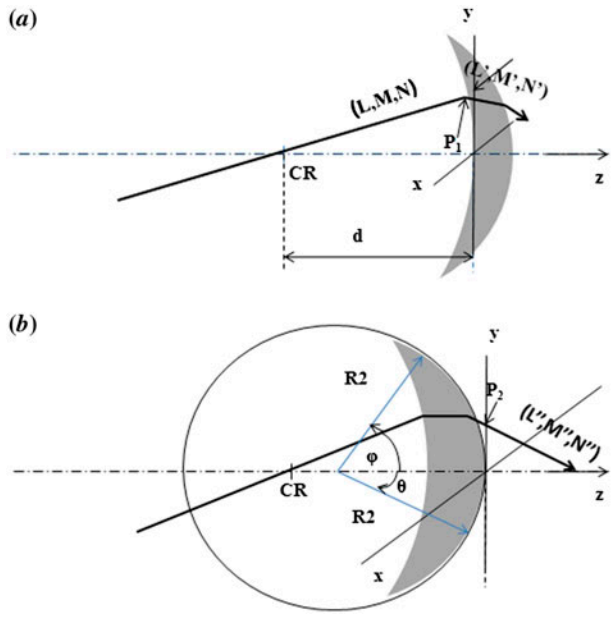

Figure A2. Finite ray tracing schematics following the notation in the text. (*a*) Magnitudes involved in tracing through the toroidal concave surface of the lens. (*b*) FRT magnitudes involved in tracing through the spherical convex surface of the lens. (The colour version of this figure is included in the online version of the journal.)

This ray is refracted by the toroidal surface, travels through the lens, and is finally refracted by the anterior spherical surface of the lens.

Let the coordinates of P_1 be (x_1, y_1, z_1). This point can be found by the intersection of the line that contains the incident ray with the toroidal surface. The line that contains the director vector of the incident ray can be parameterized relative to a coordinate system situated at the posterior vertex of the lens as:

$$x = \lambda L \quad y = \lambda M \quad z = \lambda N - d. \qquad (28)$$

The point P_1 is common to the line and the toroidal surface, so:

$$\begin{aligned} \lambda L &= (R - r + r\cos\varphi)\sin\theta \\ \lambda M &= r\sin\varphi \\ \lambda N - d &= -R + (r - r + r\cos\varphi)\cos\theta, \end{aligned} \qquad (29)$$

which becomes a system of nonlinear equations to be solved. Although different solutions may be found, we will only be interested in the minimum absolute z value. Then, the intersection point of the incident ray with the posterior surface of the lens is obtained.

The next step is thus refraction at the toroidal surface. From the vector form of Snell's law (Equation (3)), $\boldsymbol{r}$ and $\boldsymbol{r'}$ are unit vectors along the incident and refracted rays and $\boldsymbol{n}$ is a unit vector along the normal to the surface at P_1. The components of $\boldsymbol{r}$ and $\boldsymbol{r'}$ are (L, M, N) and (L', M', N'), respectively and $\boldsymbol{n}$ can be calculated using:

$$\boldsymbol{n} = (\boldsymbol{s}_\theta \times \boldsymbol{s}_\varphi)/[(\boldsymbol{s}_\theta \times \boldsymbol{s}_\varphi)^2]^{1/2}, \qquad (30)$$

where $\boldsymbol{s}_\theta$ and $\boldsymbol{s}_\phi$ are the partial derivatives of the surface S respect θ and φ at the point P_1.

This enables the following to be obtained:

$$\boldsymbol{n} = (-\sin\theta\cos\varphi), -\sin\varphi, (-\cos\theta\cos\varphi)) \tag{31}$$

In order to apply Snell's law we are interested that normal direction follows ray direction, i.e. the normal is considered to be:

$$\boldsymbol{n} = (\sin\theta\cos\varphi, \sin\varphi, \cos\theta\cos\varphi) \tag{32}$$

Using the vector form of Snell's law (Equation (7)), it is now possible to find the director cosines for the refracted ray in the posterior surface of the lens, (L', M', N')

Now, a new transfer and refraction processes for the ray crossing the lens at the anterior surface of the lens need be applied. The ray will hit the anterior surface at point P_2, with coordinates (x_2, y_2, z_2), and refracted yielding the director cosines for the refracted ray on the anterior surface of the lens (L'', M'', N'') (see Figure 3(*a*)). Both processes are entirely equivalent to the ones described in the previous paragraph, except for the fact that now the refractive surface is spherical so its parametric description in a reference system at its anterior vertex becomes:

$$s = \left\{ \begin{array}{l} x = R_2\cos\varphi\sin\theta \\ y = R_2\sin\varphi \\ z = R_2\cos\varphi\cos\theta - R_2 \end{array} \right\}, \tag{33}$$

where $0 \le \varphi \le 2\pi$ and $0 \le \theta \le 2\pi$ and again R_2 is considered in absolute value, with

$$\varphi = \arcsin(y_2/R_2) \quad \theta = \arcsin(x_2/R_2), \tag{34}$$

so the normal to the surface at the point P_2 can again be calculated:

$$\boldsymbol{n} = (\sin\theta\cos\varphi, \sin\varphi, \cos\theta\cos\varphi), \tag{35}$$

and through Equation (7) we get (L'', M'', N''). The detailed FRT equations are now complete, so the path of the principal ray has been determined. We can now proceed to the application of the GRT procedure in each case of interest.

A2. Generalized ray tracing

To implement the GRT equations we turn the system backwards to its original position and send to the lens narrow bundles of light to evaluate its performance locally. We are interested in the bundles which have as point of incidence on the anterior surface of the lens point P_2, and director cosines determined by (L'', M'', N''). Turning the system to its original position and changing the direction of incidence involves some changes in the sign in the coordinate systems (signs at the x and z coordinates), in the M director cosine and in the radius of curvature.

We start with an object at infinity, corresponding to a flat wavefront. The ray with director cosines (L'', $-M''$, N'') and point of incidence $P_2 = (-x_2, y_2, -z_2)$ is orthogonal to the incident wavefront. The refracting surface is a sphere, and its normal components at the point P_2 are known.

For the refraction on the anterior surface of the lens,

$$\mu_2 = 1/n', \tag{36}$$

and since the wavefront is plane,

$$\rho_{u2} = \rho_{v2} = 1/\sigma_2 = 0. \tag{37}$$

The refracting surface is a sphere, so it has not any principal direction, and $1/\sigma_{s2} = 0$. Moreover, if the sphere radius is $-R_2$, we may set

$$\rho_{us2} = \rho_{vs2} = -R_2. \tag{38}$$

The values of $\cos i$ and $\cos i'$ remain to be determined. We have calculated these values along the finite ray tracing process described, although now incidence and refraction angles are reversed. γ_2 can be calculated as:

$$\gamma_2 = -\mu_2\cos i + \cos i' \tag{39}$$

With this information, using Equations (24)–(26) we obtain:

$$1/\rho'_{u2} = (\gamma_2/-R_2), \tag{40}$$

$$\cos i'/\sigma'_2 = 0, \tag{41}$$

$$\cos^2 i/\rho'_{v2} = (\gamma_2/-R_2), \tag{42}$$

with ρ'_{u2} and ρ'_{v2} the refracted wavefront curvatures on the anterior surface of the lens at point P_2. The value of $1/\sigma'_2$ is zero, but the two curvatures are not equal in the general case. The fact that $1/\sigma'_2$ is zero tells, us that we are already oriented with respect to the principal directions and that the $\boldsymbol{p}_2$ vector is in the direction of one of them. In this case $\boldsymbol{p}_2 = \boldsymbol{t}_2$ because $\rho'_{u2} = \rho'_{\xi 2}$ and $\rho'_{v2} = \rho'_{\eta 2}$. So following Equation (10), the expression to find $\boldsymbol{p}_2$ is:

$$\boldsymbol{p_2} = \boldsymbol{r} \times \boldsymbol{n}/\sin i, \tag{43}$$

where the components of the incident ray $\boldsymbol{r}$ = (L'', $-M''$, N''), those of the normal to the surface at the point of incidence and the angle i are known.

The next refracting surface is the posterior surface of the lens. It's now necessary to perform a transfer operation to know how the wavefront curvatures change when the ray travels from the first surface of the lens to the second surface, i.e. from P_2 to P_1. The distance between these points can easily be calculated. Let this distance be e'. Then, when the wavefront arrives to P_1 these principal curvatures are:

$$\rho_{\xi 1} = \rho'_{\xi 2} + e', \tag{44}$$

$$\rho_{\eta 1} = \rho'_{\eta 2} + e'. \tag{45}$$

The posterior surface of the lens is a toroidal surface. The parameterization of this surface to perform the wavefront tracing, once the path of the ray has been reversed, will be

$$s = \left\{ \begin{array}{l} x = -(R - r + r\cos\varphi)\sin\theta \\ y = r\sin\varphi \\ z = R - (r - r + r\cos\varphi)\cos\theta \end{array} \right\}, \tag{46}$$

where again $0 \le \varphi \le 2\pi$ and $0 \le \theta \le 2\pi$ and R and r are considered as absolute values.

This parametric equation allows us to calculate the normal vector and the fundamental forms of the toroidal surface. The normal vector is:

$$\boldsymbol{n} = (\sin\theta\cos\varphi, -\sin\varphi, \cos\theta\cos\varphi). \tag{47}$$

The first and second Gauss fundamental forms of the toroidal surface [23] are, respectively:

$$E = (R - r + r\cos^2\varphi)$$
$$F = 0$$
$$G = r^2 \tag{48}$$

$$e = (R - r + r\cos\varphi)\cos\varphi$$
$$f = 0$$
$$g = -r \tag{49}$$

These fundamental forms enable to obtain the principal curvatures of the surface and the principal directions of the surface at the point of intersection of the ray. The principal curvatures are calculated as the eigenvalues of **A** and the principal directions as its eigenvectors, where **A** is defined by:

$$\mathbf{A} = \left(\frac{1}{EG - F^2}\begin{pmatrix} eG - fF & -eF + fE \\ fG - gF & Eg - fF \end{pmatrix}\right). \tag{50}$$

A particular coordinate system at the point of the intersection of the ray with the surface is created. With this purpose the vector $\boldsymbol{p}$ for the posterior surface of the lens at point P_1 ($\boldsymbol{p_1}$) is obtained following Equation (10):

$$\boldsymbol{p_1} = \boldsymbol{r} \times \boldsymbol{n}/\sin i, \tag{51}$$

where $\boldsymbol{r}$ = (L', $-M'$, N'), the surface normal at the point of incidence for the toroidal surface $\boldsymbol{n}$ and angle i are known. The angle between $\boldsymbol{t}_2$ and $\boldsymbol{p}_1$ can be found using:

$$\cos\theta = \boldsymbol{t}_2 \cdot \boldsymbol{p_1}, \tag{52}$$

where $\boldsymbol{t_2}$ defines a principal direction of the incident wavefront to the surface at the point of incidence.

Finally, two rotations are performed using Equations (17)–(19) to find the curvature of the wavefront (ρ_{u1}, $\rho_{\varpi 1}$) and the curvature of the refractive surface (ρ_{u1s}, ρ_{v1s}) at the direction of $\boldsymbol{p}_1$. For the refraction at the posterior surface of the lens:

$$\mu_1 = n', \tag{53}$$

$$\gamma_1 = -\mu_2\cos i + \cos i'. \tag{54}$$

With this information, Equations (24)–(26) can be applied again to obtain the values ρ'_{u1} and ρ'_{v1}, which are the refracted curvatures of the wavefront in the direction of $\boldsymbol{p}_1$ and $\boldsymbol{q}_1$, respectively.

The principal curvatures of the refracted wavefront through the lens can now be obtained from Equations (20)–(22). Firstly, the angle between $\boldsymbol{p}_1$ and $\boldsymbol{t'}_1$ is obtained from Equation (22). Then, the principal curvatures are obtained from Equations (20) and (21). These curvatures are ρ'_ξ and ρ'_η, and the direction of $\boldsymbol{t'}_1$ is obtained from Equation (23).

As a last step, the curvatures of the refracted wavefront have to be defined relative to a reference surface which is the same regardless the geometry of the posterior surface of the lens, to avoid ambiguities. This reference surface is called the vertex sphere, a spherical surface centered at the center of rotation of the eye whose radius is the distance from the back vertex of the lens to the center of rotation of the eye.

The refracted wavefront curvatures are then calculated when they intersect this vertex sphere. The distance from the back surface of the lens to the vertex surface for each ray is calculated, and the refracted wavefront curvatures properly modified similarly to the previously described transfer procedure (Equations (44) and (45)). The position of the centers of curvature for the principal curvatures of the refracted wavefront associated with each particular ray is interpreted as the equivalent to the sagital and tangential focus in the classical Coddington equations.